C. R. Palevol 15 (2016) 163–175

Contents lists available at ScienceDirect

Comptes Rendus Palevol

www.sciencedirect.com

General Palaeontology, Systematics and Evolution

Bone histology and growth in *Stenaulorhynchus stockleyi* (Archosauromorpha: Rhynchosauria) from the Middle Triassic of the Ruhuhu Basin of Tanzania

Histologie osseuse et mode de croissance chez Stenaulorhynchus stockleyi *(Archosauromorpha : Rhynchosauria) du Trias moyen du bassin Ruhuhu de Tanzanie*

Sarah Werning[a,*], Sterling J. Nesbitt[b]

[a] *Department of Anatomical Sciences, Stony Brook University, Stony Brook, NY 11794, USA*
[b] *Department of Geosciences, Virginia Polytechnic and State University, Blacksburg, VA 24061, USA*

ARTICLE INFO

Article history:
Received 1st December 2014
Accepted after revision 11 March 2015

Handled by Michel Laurin

Keywords:
Archosauria
Paleohistology
Histological variation
Growth rates
Gondwana

ABSTRACT

The bone histology of non-archosauriform archosauromorphs is understudied but is important for tracing the evolution of growth in archosaurs and their closest relatives. Here, we describe the femoral and tibial histology of a single individual of *Stenaulorhynchus stockleyi*, a Middle Triassic rhynchosaur from Tanzania. Both elements are composed largely of moderately vascularized parallel-fibered bone tissue, which becomes avascular and more lamellar approaching the periosteum. The spacing between growth marks in *S. stockleyi* strongly attenuates with age, suggesting determinate growth for this taxon. Whereas the bone tissue suggests slower growth compared to South American rhynchosaurs, which have fibrolamellar bone tissue and exhibit more anastomoses between canals, the determinate growth pattern seems to be shared among hyperodapedontid rhynchosaurs. Although non-archosauriform archosauromorphs vary in the rate of bone deposition and growth in their first year, all taxa examined to date grew relatively slowly compared to most archosauriforms.

Mots clés :
Archosauria
Paléohistologie
Variation histologique
Taux de croissance
Gondwana

RÉSUMÉ

L'histologie osseuse d'archosauromorphes non archosauriformes est mal connue par rapport à celle des archosauriformes, en particulier à celle des archosauriens Orthodira (ancêtres des oiseaux). Nous décrivons ici l'histologie du fémur et du tibia d'un unique individu de *Stenaulorhynchus stockleyi*, un rhynchosaurien du Trias moyen de Tanzanie. Ces deux éléments sont en grande partie constitués de tissu osseux en fibres parallèles, modérément vascularisé, qui devient non vascularisé et plus lamellaire à l'approche du périoste. L'espacement entre les marques de croissance chez *S. stockleyi* s'atténue fortement avec l'âge, ce qui suggère une croissance déterminée dans ce taxon. Alors que le tissu osseux suggère une croissance plus lente par rapport à celle observée chez les rhynchosauriens

* Corresponding author.
E-mail address: sarah.werning@stonybrook.edu (S. Werning).

http://dx.doi.org/10.1016/j.crpv.2015.03.004
1631-0683/

d'Amérique du Sud, qui ont tissu osseux fibro-lamellaire et présentent un plus grand nombre d'anastomoses entre les canaux, le schéma de croissance déterminée semble être partagé parmi les rhynchosauriens hypérodapédontidés. Bien que le taux de dépôt d'os et de croissance soit variable chez les archosauromorphes non archosauriformes au cours de leur première année, tous les taxons examinés jusqu'à présent ont une croissance relativement lente, comparée à celle de la plupart des archosauriformes.

1. Introduction

The bone microstructure of archosaurs and their extinct relatives has been a ripe area of study for paleohistologists in general (e.g., Botha-Brink and Smith, 2011; Enlow, 1969; Enlow and Brown, 1957; Gross, 1934; Horner et al., 2001; Peabody, 1961; Seitz, 1907) and French paleohistologists in particular (e.g., Cubo et al., 2012; de Buffrénil et al., 2015; de Ricqlès, 1976; de Ricqlès et al., 2003, 2008). Much recent work in this field has focused on the origin and evolution of avian growth rates and thermophysiology. As a result, the long bone histology of bird-line (ornithodiran) archosaurs (e.g., Chinsamy et al., 1995; Cubo et al., 2012; Griffin and Nesbitt, In revision; Nesbitt et al., 2013; Werning et al., 2011) is much better characterized in both number of taxa and phylogenetic breadth compared to that of crocodile-line (pseudosuchian) archosaurs. Outside the crown, several studies have suggested that many of the histological features associated with elevated growth and metabolic rates were already present among the Archosauriformes (= stem archosaurs; e.g., Botha-Brink and Smith, 2011; Cubo et al., 2012; Legendre et al., 2013; Scheyer et al., 2014; Werning, 2013; Werning et al., 2011).

Few studies have examined the long bone histology of non-archosauriform archosauromorphs, but this region of the saurian phylogenetic tree (Fig. 1A) is important for establishing the plesiomorphic conditions of tissue structure, growth rate, metabolism, and thermophysiology for Archosauromorpha (after the split with lepidosauromorphs, including squamates and rhynchocephalians). In those early diverging archosauromorph taxa that have been characterized, the bone tissue structure generally suggests slower growth compared to archosauriforms, with most taxa exhibiting moderately to poorly vascularized parallel-fibered or lamellar bone (Botha-Brink and Smith, 2011; de Ricqlès et al., 2008; Ezcurra et al., 2014; Veiga et al., in press; Werning and Irmis, 2011). However, with two exceptions (Mukherjee, 2015; Werning and Irmis, 2011), no taxon has been sampled in large enough numbers to address ontogenetic variation in growth or histology. Greater sampling among non-archosauriform archosauromorphs is necessary to understand the distribution of and variation in growth-related histological features.

An ideal clade on which to focus sampling efforts is Rhynchosauria, a group of non-archosauriform archosauromorphs restricted to the Triassic. Rhynchosaurs represent one of the earliest groups of archosauromorphs to reach a nearly Pangean distribution (Benton, 1983, 1984; Dilkes, 1995, 1998). Not only were rhynchosaurs widely distributed and rather common in the southern portion of Pangea, but they were the first large reptiles (up to 2 m in length) to appear in the Triassic fossil record with craniofacial adaptations for herbivory (Dilkes, 1995). Well supported phylogenies of rhynchosaur interrelationships (Dilkes, 1995, 1998; Montefeltro et al., 2010, 2013) found that most craniodental features indicative of herbivory clearly originated before increases in body size; yet, the process of this change has not been documented in detail.

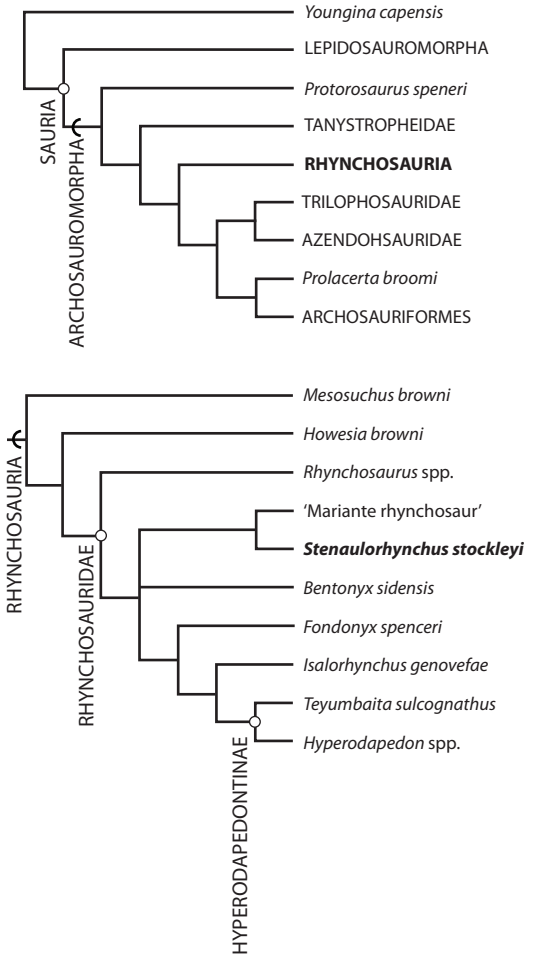

Fig. 1. The phylogenetic *positions* of A) rhynchosaurs among early saurians, and of B) *Stenaulorhynchus stockleyi* among the members of Rhynchosauria. Relationships from Nesbitt et al. (in revision) and Montefeltro et al., 2013. Circle = node group, chevron = stem group.

Fig. 1. Positions phylogénétiques des rhynchosauriens (A) parmi les premiers sauriens et de *Stenaulorhynchus stockleyi* (B) parmi les membres des Rhynchosauria. Relations phylogénétiques selon Nesbitt et al. (sous révision) et Montefeltro et al., 2013. Cercle = groupe de nœuds, chevron = groupe de la tige.

Furthermore, both Late Triassic (Chatterjee, 1974; Veiga et al., in press) and Middle Triassic (unpublished specimens of *Stenaulorhynchus*) taxa are known from at least a partial growth series.

Despite this potential, the bone histology of rhynchosaurs is not thoroughly described. Enlow and Brown (1957) and Enlow (1969) first described the rib microstructure of *Hyperodapedon sanjuanensis* (then *Scaphonyx sanjuanensis*). Armand de Ricqlès (1976) also commented on the rib histology of *Hyperodapedon* (then *Scaphonyx*), but the sections were not illustrated or described in detail until a later work (de Ricqlès et al., 2008). More recently, a *Stenaulorhynchus* limb bone was illustrated by Sanchez et al. (2012), but was not described histologically. To date, the only studies to focus on rhynchosaur osteohistology are that of Veiga et al. (in press), who sectioned long bones and ribs of a *Hyperodapedon* species and *Teyumbaita sulcognathus*, both from Brazil, and Mukherjee (2015), who sectioned long bones from the Indian rhynchosaurs *H. huxleyi* and *H. tikiensis*, including a femoral growth series. Although the Late Triassic hyperodapedontine rhynchosaurs are now well sampled, little is known about growth in earlier diverging rhynchosaurs, or whether these forms are representative of the entire clade.

Here, we present new histological data on the Middle Triassic rhynchosaur *S. stockleyi*, based on the midshafts of a femur and tibia from a single individual. Each bone appears to preserve nearly the entire ontogenetic growth record. *Stenaulorhynchus* is an excellent candidate for histological study because it is known from associated crania and postcrania of various size classes. Additionally, *Stenaulorhynchus* is one of the earliest large-bodied rhynchosaurs (> 1 m in length), a size on par with that of Late Triassic rhynchosaurs.

2. Materials and methods

2.1. Institutional abbreviations

MCZ (Museum of Comparative Zoology, Harvard University, Cambridge, MA, USA); NHMUK (Natural History Museum, London, United Kingdom); NMT (National Museum of Tanzania, Dar es Salaam, Tanzania); SAM (Iziko South African Museum, Cape Town, South Africa); UFRGS (Universidade Federal do Rio Grande do Sul, Porto Alegre, Rio Grande do Sul, Brazil).

2.2. Specimen and locality information

We sampled the mid-diaphyses of a left femur and right tibia (Fig. 2A, C) from a single individual of *S. stockleyi*, NHMUK PV R 36618 (field number U2/26). This specimen was collected in 1963 by the British Museum (Natural History) – University of London Joint Paleontological Expedition from the Middle Triassic (?Late Anisian) Manda beds in the Ruhuhu Basin, Songea District, Tanzania (Triassic locality 2; see Cox, 1991, Text – Fig. 1 for map). According to collection notes made by Alan Charig (NHMUK unpublished fieldnotes), the femur and tibia were collected together with "various pieces of *Stenaulorhynchus*, including excellent vertebrae, not necessarily associated". However, the specimen includes contralateral elements of identical size (tibiae, humeri, calcanea) and preserves no duplicate elements, suggesting a single individual (SW, pers. obs.).

The morphology and proportions of the limb elements are consistent with that of *S. stockleyi* (*sensu* von Huene, 1938), but femoral and tibial autapomorphies for this species are not yet known. Among the preserved elements is a right maxilla, which can be assigned to *S. stockleyi* based on the presence of the following character states: lingual teeth present, teeth bulbous, and three rows of anteroposteriorly aligned teeth separated by deep grooves (SJN, pers. obs.). Like the assignment of NHMUK PV R 36618 to *S. stockleyi*, the limb elements by themselves cannot be unambiguously assigned to Rhynchosauria because most of the informative character states supporting the monophyly of and interrelationships among rhynchosaurs derive from the skull. However, they are consistent with the hindlimb morphology of larger rhynchosaurs (e.g., *T. sulcognathus*, Montefeltro et al., 2013): they are robust and have a large internal trochanter and similar epiphyseal expansions.

Stenaulorhynchus is in need of a complete revision because the holotype (SAM 10651, Stockley number S340) represents a mixed assemblage (rhynchosaur postcrania with archosaur maxillae; Haughton, 1932) and there is a great deal of undescribed material. However, it appears that there is only one large rhynchosaur from the Lifua Member of the Manda beds, as all of the cranial material, including the maxillary tooth plates, are similar in morphology. Therefore, we use *Stenaulorhynchus* in the sense of von Huene's (1938) description of referred material of *Stenaulorhynchus*, based on associated skeletons (some articulated) and skulls with maxillae.

2.3. Histological preparation

SW prepared histological slides using the methods Lamm (2013) described for fossil bone. Prior to sectioning, we photographed, molded, and cast both elements to preserve the original morphology; these are reposited at NHMUK. Images of these elements pre-sectioning are available on MorphoBank (list of images in SOM; http://morphobank.org/permalink/?P1245; O'Leary and Kaufman, 2012), Project P1245. We removed the mid-diaphyses and embedded them in Silmar-41 clear polyester resin (US Composites, West Palm Beach, FL, USA) catalyzed with methyl ethyl ketone peroxide at 1% by mass. The resin cured at room temperature for at least 72 hours before sectioning on an IsoMet 1000 precision saw (Buehler, Lake Bluff, IL, USA). Sections were serially cut at 1.5–2 mm intervals and mounted to glass slides using clear Devcon® 2 Ton® Epoxy (ITW Polymers Adhesives, Danvers, MA, USA). Slides were ground using progressively finer silicon carbide grit papers on a P30F-1-HA grinder-polisher (Precision Surfaces International, Houston, TX, USA). Preparation records are on file at NHMUK.

2.4. Histological imaging

Slides were imaged dry and wet with water to increase light penetration. To create digital cross-sections, we took overlapping images of each slide with a QICClick F-CLR-12 digital camera (QImaging, Surrey, BC, Canada) mounted to a

DMRXE transmitted light microscope (Leica Microsystems, Wetzlar, Germany), using either a single polarizing filter or under circularly polarized light. Photomosaics were assembled using Surveyor version 7.0.0.7 (Objective Imaging Inc., Kansasville, WI, USA). We adjusted the images (leveling, adding scale bars) and traced the growth marks and periosteum in Photoshop CS6 Extended (Adobe Systems Inc., San Jose, CA, USA). High-resolution images of these sections are available on MorphoBank.

2.5. Measurements

External measurements of the sampled femur and tibia were obtained using an 8-inch digital caliper (Neiko Tools, China) and a tailor's soft measuring tape (Amico, Richmond Hill, ON, Canada). We took histological measurements from digital cross-sections T2 and Fe3 using Photoshop CS6 Extended. Mid-diaphyseal and medullary cavity diameter were measured along their respective major and minor axes using Ruler Tool. Zonal widths were measured along the cross-sectional major axis (widest width of section) and minor axis (shortest height of section perpendicular to major axis). Sectional axes are visible in MorphoBank images M346027 and M346740. Generally this produced four measurements, which were averaged. Because the externalmost growth marks are only partially preserved, the zonal widths between them were measured as close to a major or minor axis as possible, along a radius extending from the intersection of the major and minor axes. All measurements are reported in Table 1.

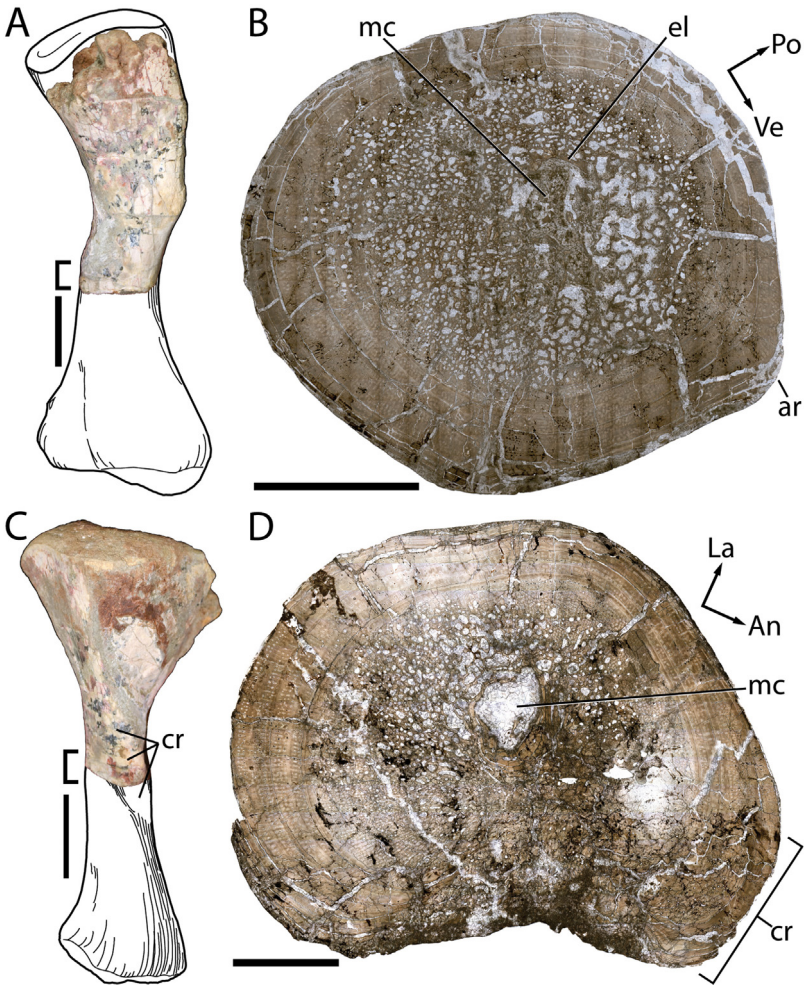

Fig. 2. (Color online.) Left femur (A, B) and right tibia (C, D) of *Stenaulorhynchus stockleyi* (NHMUK PV R 36618). A. Sectioned femur in dorsal view, with missing portions reconstructed based on von Huene (1938). B. Femoral cross-section at mid-diaphysis. C. Sectioned tibia in anterior view with missing portions reconstructed based on von Huene (1938). D. Tibial cross-section at mid-diaphysis. Brackets indicate regions sampled for histological study. Scales: A, C = 3 cm; B = 10 mm; D = 5 mm. Abbreviations: ar: adductor ridge; An: anterior; cr: anterior crest; el: endosteal lamellae; La: lateral; mc: medullary cavity; Po: posterior; Ve: ventral.

Fig. 2. (Couleur en ligne.) Fémur gauche (A, B) et tibia droit (C, D) de *Stenaulorhynchus stockleyi* (NHMUK PV R 36618). A. Coupe de fémur en vue dorsale, avec les parties manquantes reconstituées d'après von Huene (1938). B. Section transversale du fémur à mi-diaphyse. C. Coupe de tibia en vue antérieure, avec les parties manquantes reconstituées d'après von Huene (1938). D. Section transversale du tibia à mi-diaphyse. Les crochets indiquent les zones échantillonnées pour l'étude histologique. Échelles : A, C = 3 cm ; B = 10 mm ; D = 5 mm. Abréviations : ar : crête adductrice ; An : antérieure ; cr : crête antérieure ; el : lamelles endostéales ; La : latérale ; mc : cavité médullaire ; Po : postérieure ; Ve : ventrale.

Table 1
Linear measurements of the sampled left femur and right tibia of *Stenaulorhynchus stockleyi* (NHMUK PV R 36618). All measurements are in mm.
Tableau 1
Mesures linéaires du fémur gauche et du tibia droit de *Stenaulorhynchus stockleyi* (NHMUK PV R 36618). Toutes les mesures sont en mm.

Measurement	Left Femur	Right Tibia
Total proximal-distal length	182	–
Proximal width	80	75
Distal width	79	50
Distance from proximal end to the mid-diaphysis	99	85
Mid-diaphyseal circumference	102	79
Mid-diaphyseal width (major × minor axis)	33.65 × 29.76	25.95 × 23.98
Medullary cavity width (major × minor axis)	4.9 × 4.5 (estimated)	4.28 × 2.95

For each element, we estimated daily bone deposition rates for the three main phases of growth (recorded year 1, years 2–5, years 6–12). The tissue between adjacent annual lines of arrested growth or annuli represents all the bone deposited in that year. For extant species, daily [radial] bone deposition rates are estimated by dividing the width of this zone by the number of days in the known growth season (e.g., Castanet, 1985). In extinct taxa, the duration of the growth season is unknown and requires estimation. One approach is to estimate minimum bounds for daily growth under the assumption that the growth season lasted an entire year, but this method underestimates actual daily rates by a considerable amount if the growth season occurred in a small window of time (Botha-Brink and Smith, 2011; Castanet and Baez, 1991). Therefore, we estimated daily bone deposition under four hypothetical growth durations: 383 days (the estimated length of a Middle Triassic year; Wells, 1963), 365 days, 270 days, and 180 days (corresponding to a modern year, nine month, and six month growth season, respectively). For the first year of growth, we calculated two sets of rates, assuming a neonatal [geometric] radius of 2.5 mm or 5 mm for each element. Calculations are reported in the Supplemental Online Material (SOM).

3. Results

3.1. Histological descriptions

We use the osteohistological terminology of Francillon-Vieillot et al. (1990), the bone orientation terminology of Gower (2003), and the phylogenetic relationships of Nesbitt et al. (in revision) and Montefeltro et al. (2013). We describe general features of the cross-section first, then discuss aspects of the microstructure in detail, moving from the endosteal margin to the periosteal surface. Numbers in parentheses beginning with "M" (e.g., M339571) denote specific images on MorphoBank.

3.1.1. Femur

The mid-diaphyseal section of the femur is subcircular in cross-section, with the adductor ridge (= internal trochanter, the hypothesized attachment location of the caudofemoralis musculature) visible as a small triangular projection between the ventral and posterior faces (Fig. 2B, ar). The endosteal margin is difficult to discern in this slide because of taphonomic trabecular fracturing, but in other slides and cut blocks, a distinct subrectangular medullary cavity lies slightly off center (Fig. 2B, mc; M339571, M346024). Cancellous bone comprises almost two thirds of the bone's diameter, but does not reach the growth marks except in the anterodorsal quadrant, where they extend past the third line of arrested growth (LAG). The compact cortical bone is fairly even in thickness around the section, but is slightly thinner dorsally.

The endosteal lamellae (Fig. 2B, el) form a band 2–3 times thicker than the trabeculae of the innermost cortex. The trabeculae clearly formed through the resorption of primary compact bone, which is still visible between erosion rooms especially in the posterior quadrant (Fig. 3D). Endosteally, erosion rooms are irregular or oval and closely spaced, and become rounder and farther spaced periosteally. They are largest in the posteroventral quadrant. Each erosion room is lined by one to three lamellae of irregular thickness.

The compact cortex is primarily composed of primary parallel-fibered bone tissue internal to the fifth LAG (Fig. 3B, C; M346720; M346722), with lamellar bone external to the fifth LAG and flanking the growth marks. Internal to the first LAG, several bands of very distinct lamellae are visible in the posterior quadrant, which at low magnification resemble part of a multiple LAG. When viewed under polarized light or when focused through at higher magnification, it is clear that there are no tissue discontinuities, so they cannot be a multiple LAG. It is possible these bands represent an annulus, but they do not continue very far circumferentially. Additionally, the tibia preserves more primary bone in the cancellous region and has no equivalent bands, despite an otherwise identical distribution of growth marks (see below). Therefore, we hypothesize that the internal most LAG likely represents the first LAG deposited.

Twelve definitive cortical growth marks are preserved (Fig. 3A shows ten; M337274). The inner three are LAGs that locally become double or multiple LAGs (Fig. 3A, note arrows). The fourth is an annulus of lamellar bone with only local, short breaks in tissue. The outermost eight are closely spaced LAGs at the periphery of the bone; these are incompletely preserved around the periosteal circumference because of surface abrasion. The spacing of these seven zones is fairly consistent and the lamellar bone between them is largely avascular, so we interpret them as an external fundamental system (EFS) or outer circumferential layer (Fig. 3A, efs; M337274). The zones between growth marks are slightly wider approaching the adductor ridge.

In regions of parallel-fibered bone, the elongate osteocytes are arranged more or less circumferentially, but are irregularly spaced. In areas of lamellar bone, they are spaced more regularly and line up along lamellae.

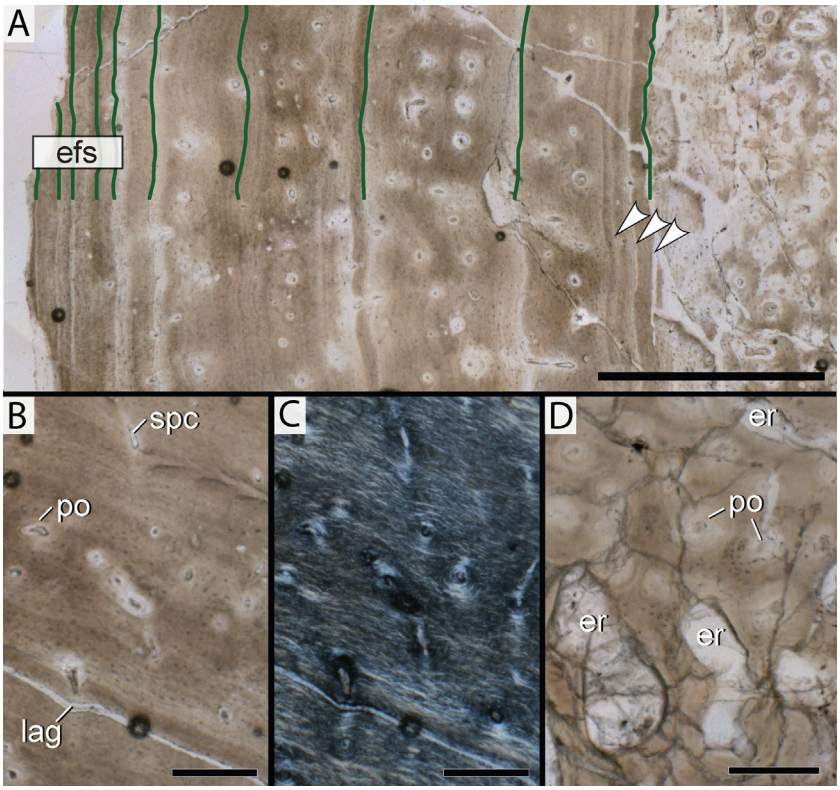

Fig. 3. (Color online.) Mid-diaphyseal microstructure of the femur of *Stenaulorhynchus stockleyi* (NHMUK PV R 36618) in single plane polarized light (A, B, D) and circularly polarized light (C). A. Radial transect across-section Fe1 showing the first ten growth marks (vertical lines). In this region, the innermost LAG is a triple LAG (three arrows); elsewhere they merge into a single LAG. Canal density and growth line spacing both decrease moving periosteally (to left of image). The outer two growth marks are not preserved in this region of the cortex because of surface abrasion. B. Close-up of the middle cortex of section Fe1 (between LAGs 3 and 4), showing variation in vascular canal type. C. Same region as (B) in circularly polarized light to highlight parallel-fibered bone. D. Inner cortex of section Fe2 showing primary tissues preserved between erosion rooms. Abbreviations: efs: external fundamental system; er: erosion room; lag: line of arrested growth; po: primary osteon; spc: simple primary canal. Scales: A = 1 mm; B, C, D = 250 μm.

Fig. 3. (Couleur en ligne.) Microstructure mi-diaphysaire du fémur de *Stenaulorhynchus stockleyi* en lumière polarisée plane (A, B, D) et en lumière polarisée circulairement (C). A. Transect radial à travers la section Fe1, montrant les dix premières marques de croissance arrêtée (lignes verticales). Dans cette région, la LAG la plus profonde est une LAG triple (trois flèches) ; ailleurs elles fusionnent en une seule ligne. La densité des canaux et l'espacement entre les lignes de croissance diminuent à l'approche du périoste (à gauche de l'image). Les deux marques de croissance externe ne sont pas conservées dans cette zone du cortex, du fait de l'abrasion de surface. B. Gros plan du cortex médian de la coupe Fe1 (entre les LAGs 3 et 4), montrant la variation dans le canal vasculaire type. C. Même zone que (B) en lumière polarisée circulairement pour mettre en évidence l'os à fibres parallèles. D. Cortex interne de la coupe Fe2 montrant les tissus primaires conservés entre les espaces érodés. Échelles : A = 1 mm ; B, C, D = 250 μm. Abréviations : efs : système externe fondamentale ; er : espace d'érosion ; lag : ligne de la croissance arrêtée ; po : ostéone primaire ; spc : canal primaire simple.

Endosteally, the osteocytes orbit vascular canals, but external to the third LAG, they do not (Fig. 3B; M346721; M346723).

Internal to the first LAG, the bone is moderately vascularized by longitudinal or slightly oblique primary osteons arranged in radial rows. Between the first and fifth LAGs, the distance between canals increases (Fig. 3A). This is especially noticeable in the posterodorsal quadrant, where they are arranged circumferentially or randomly rather than in radial rows. In this quadrant, about half of the canals are simple primary canals; elsewhere they comprise less than a quarter. External to the seventh LAG, the bone is nearly avascular. Anastomoses are rare throughout the section, but are slightly more common towards the adductor ridge. When present, they connect two canals radially. Secondary osteons are rare and only present internal to the first LAG; most secondary remodeling occurs in the form of erosion rooms.

3.1.2. Tibia

The mid-diaphyseal tibia is kidney-shaped in cross-section, with a small, subelliptical or V-shaped medullary cavity that sits centrally (Fig. 2D, mc). This odd cross-sectional shape results from a crest that runs diagonally across the anterior face of the tibial shaft (the "tibial crest" of Montefeltro et al., 2013; Fig. 2C, D, cr); without it, the bone would be oval in cross-section. Cancellous and compact bone each comprises about half the radius except anteriorly, where the bone is nearly all compact. As in the femur, the innermost tibial LAG lies just outside the transition from cancellous to compact bone. In slide T2, only three erosion rooms are visible external to the first LAG (Fig. 2D), and in slide T1 (M339657) none cross it. Overall, the bone tissue is very similar to that of the femur.

A thick, irregular band of endosteal lamellae is visible in each section (M339657). Anteroventrally, the band is at least five times thicker than on the opposite side of

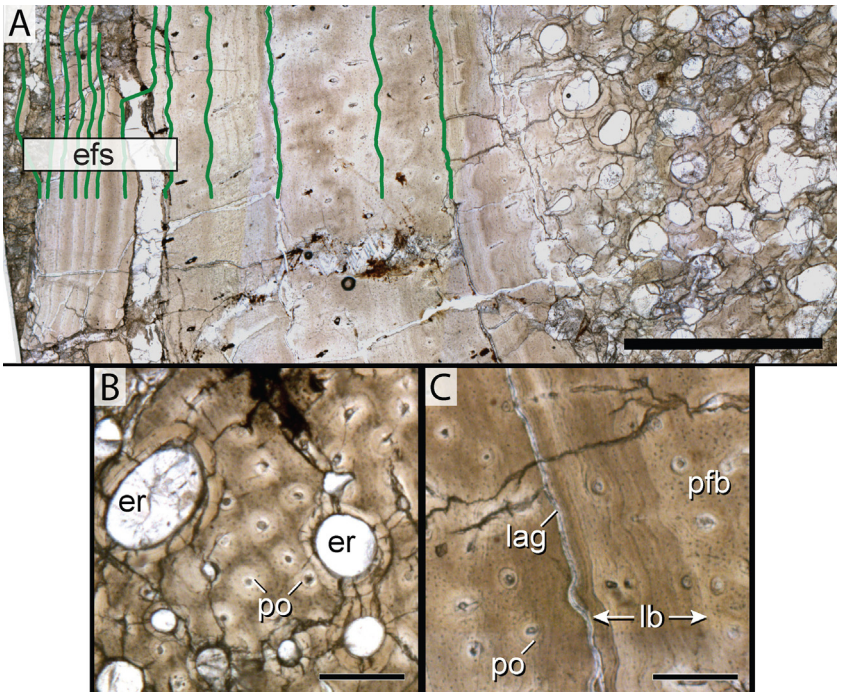

Fig. 4. (Color online.) Mid-diaphyseal microstructure of the tibia of *Stenaulorhynchus stockleyi* (NHMUK PV R 36618, section T2) in single plane polarized light. A. Radial transect showing the transition from cancellous to compact bone, growth marks (vertical lines), and the EFS. Canal density and growth line spacing both decrease moving periosteally (to left of image). B. Inner cortex, showing primary tissues preserved between erosion rooms. The primary osteons are arranged circumferentially and in radial rows (periosteum to upper right of image). C. Mid-cortex showing decrease in vascular canal density external to LAG 3 (periosteum to upper right of image). On the right side of this image, a zone of lamellar bone lies immediately outside of the LAG. The rest of this zone is composed of parallel-fibered bone. Scales: A = 1.25 mm; B, C = 250 μm. Abbreviations: efs: external fundamental system; er: erosion room; lag: line of arrested growth; lb: lamellar bone; pfb: parallel-fibered bone; po: primary osteon.

Fig. 4. (Couleur en ligne.) Microstructure à mi-diaphyse du tibia de *Stenaulorhynchus stockleyi* (NHMUK PVR 36618 ? coupe T2) en lumière polarisée régulière. A. Transect radial à travers la coupe, montrant la transition du tissu osseux de spongieux de à compact, les marques de croissance (lignes verticales) et le système externe fondamental (EFS). La densité des canaux et l'espacement entre les marques de croissance diminuent vers le périoste (à gauche de l'image). B. Cortex interne montrant les tissus primaires conservés entre les espaces érodés. Les ostéones primaires sont disposés sur la circonférence et en rangées radiales (périoste en haut à droite de l'image). C. Cortex médian montrant la diminution de la densité en canaux vasculaires à l'extérieur de la LAG 3 (périoste en haut à droite de l'image). Sur le côté droit de cette image, une zone d'os lamellaire est immédiatement à l'extérieur de la ligne de croissance arrêtée. Le reste de cette zone est composé de tissu osseux à fibres parallèles. Échelles : A = 1,25 mm ; B, C = 250 μm. Abréviations : efs : système externe fondamental ; er : espace d'érosion ; lag : ligne de la croissance arrêtée ; lb : tissu osseux lamellaire ; pfb : tissu osseux à fibres parallèles ; po : ostéon primaire.

the medullary cavity. In every slide, several oval erosion rooms pierce the endosteal lamellae; these may be lined or unlined. Within the cancellous bone, erosion rooms are largest and most irregular posteriorly. Dorsally and ventrally, they are circular or elliptical, with their long axes oriented radially (Fig. 4A). The size and density of erosion rooms decreases periosteally. As in the femur, the trabeculae formed by resorption of the primary compacta, and the original tissue is clearly visible between adjacent erosion rooms (Fig. 4B). Because the erosion rooms are smaller and unevenly distributed around the tibial circumference, more of the original compact tissue remains than in the femur.

The appearance and organization of collagen fibers and osteocytes, as well as the number, type, and relative spacing of the cortical growth marks are nearly identical to that of the femur. The only exception is the second growth mark, which is an annulus of lamellar bone for much of the tibial circumference rather than a LAG. The expansion of the anterior crest is greatest external to the fourth preserved growth mark (M339660); after this point, radial growth in the anterior direction exceeds radial growth elsewhere around the circumference.

The primary tissues internal to the first LAG are much better vascularized compared to the more external tissues. All canals are longitudinal primary osteons and they are arranged in a strong radial pattern. Anastomoses are extremely rare and only occur in the lateral quadrant, where they connect several canals radially. External to the first LAG, the primary osteons are arranged in two or three circumferential rows. Posteroventrally, a secondary signal of radial rows is visible between the first and fifth LAGs. External to the fifth LAG, the bone is avascular, except near the anterior crest; as for the femur, we interpret this region as an EFS (Fig. 4A).

3.2. Periosteal bone deposition rates

Radial periosteal bone deposition rates are reported in Table 2 (see SOM for raw data). In both elements, the highest growth rates occurred in the first year (i.e., internal to the first LAG). These rates range from 14.78–45.33 μm/d

Table 2
Radial bone deposition rates in the femur and tibia of *Stenaulorhynchus stockleyi* (NHMUK PV R 36618) under several potential growth season durations: 383 days (the hypothesized length of a Middle Triassic year; Wells, 1963), 365 days (modern year), 270 days, and 180 days. For year 1, estimates are given assuming each bone had a radius of 2.5 or 5.0 mm as a neonate. In both elements, parallel-fibered bone is the main type of bone tissue deposited through year 5, and lamellar bone is deposited in years 6-12. Abbreviation: r(neo), radius of neonate element.
Tableau 2
Taux de dépôt osseux radial dans le fémur et le tibia de *Stenaulorhynchus stockleyi* (NHMUK PV R 36618), au cours de plusieurs durées potentielles de la saison de croissance : 383 jours (durée hypothétique d'une année au Trias moyen ; Wells, 1963), 365 jours (année moderne), 270 jours et 180 jours. Pour l'année 1, les estimations sont données en supposant que chaque os a un rayon de 2,5 ou 5,0 mm comme un nouveau-né. Dans les deux éléments, l'os à fibres parallèles est le principal type de tissu osseux déposé en 5 ans, et l'os lamellaire, celui qui se dépose en 6 à 12 ans. Abréviation : r(neo), rayon de l'os nouveau-né.

	Annual growth	Growth duration = 383 d/year	Growth duration = 365 d/year	Growth duration = 270 d/year	Growth duration = 180 d/year
Femur					
Year 1, r (neo) = 2.5 mm	8160 μm/year	21.31 μm/d	22.36 μm/d	30.22 μm/d	45.33 μm/d
Year 1, r (neo) = 5 mm	5660 μm/year	14.78 μm/d	15.51 μm/d	20.96 μm/d	31.44 μm/d
Years 2–5 (mean)	1000 μm/year	2.61 μm/d	2.74 μm/d	3.70 μm/d	5.56 μm/d
Years 6–12 (mean)	160 μm/year	0.42 μm/d	0.44 μm/d	0.59 μm/d	0.89 μm/d
Tibia					
Year 1, r (neo) = 2.5 mm	6480 μm/year	16.92 μm/d	17.75 μm/d	24.00 μm/d	36.00 μm/d
Year 1, r (neo) = 5 mm	3980 μm/year	10.39 μm/d	10.90 μm/d	14.74 μm/d	22.11 μm/d
Years 2–5 (mean)	630 μm/year	1.65 μm/d	1.73 μm/d	2.33 μm/d	3.50 μm/d
Years 6–12 (mean)	150 μm/year	0.39 μm/d	0.41 μm/d	0.56 μm/d	0.83 μm/d

in the femur and 10.39–36.00 μm/d in the tibia (depending on the estimated length of the growth season), and, as a result, two thirds of total bone deposition occurred during the first year of growth (SOM). In both elements, bone deposition rates in the first year are seven to ten times higher than those of the second through fifth years (femur: 2.61–5.56 μm/d; tibia: 1.65–3.50 μm/d). In the final seven years of growth, less than a micron of bone was deposited per day, regardless of element or the growth duration assumed. In both elements, parallel-fibered bone is the main type of bone tissue deposited through year 5, and lamellar bone is deposited in years 6–12.

4. Discussion

4.1. Bone deposition rates and growth duration in *Stenaulorhynchus*

To evaluate which growth duration (180, 270, 365, or 383 d/yr) is most reasonable for *Stenaulorhynchus*, we compared estimated periosteal bone deposition rates during the time of fastest growth to known deposition rates from extant animals. In primary bone tissue, periosteal deposition rates vary with collagen fiber orientation; tissues with disorganized fibers (i.e., woven-fibered bone and fibrolamellar bone) are deposited more rapidly than more organized tissues (parallel-fibered bone and lamellar bone; Castanet et al., 2000a,b; de Buffrénil and Pascal, 1984; de Margerie et al., 2002; Enlow, 1969; Montes et al., 2010; Newell-Morris and Sirianni, 1982). Parallel-fibered bone is the most disorganized tissue observed in *Stenaulorhynchus*; it is the only bone tissue type deposited in the first five years of growth when zones are widest. We summarize parallel-fibered bone growth rates for the major long bones (humeri, femora and tibiae) of extant and extinct tetrapods in Table 3.

In the first year of growth, estimated deposition rates for the *Stenaulorhynchus* femur and tibia exceed known deposition rates for parallel-fibered bone when a growth duration of 180 days and a neonate radius of 2.5 mm are assumed. If a neonate radius of 5 mm is used, estimated rates for this growth duration are similar to those observed in the mallard, *Anas platyrhynchos*; about 30 μm/d (de Margerie et al., 2002). In the mallard, such high deposition rates were only reported for parallel-fibered bone vascularized by primary osteons, which is the case internal to the first LAG in *Stenaulorhynchus*. In years 2–5, bone depositions rates for *Stenaulorhynchus* are comfortably within known bone deposition rates for extant taxa, regardless of which growth duration is assumed. These rates are most similar to those of *Proterosuchus* (sensu Botha-Brink and Smith, 2011), *Alligator*, and mammals. Thus, known bone deposition rates for parallel-fibered cannot be used to reject any of these growth durations, unless a very small neonate radius is assumed.

Periosteal bone growth rates are strongly influenced by body mass, metabolism, and ontogenetic stage; they also vary by taxon, by element, and with resource availability (de Buffrénil and Pascal, 1984; Castanet, 1985; Castanet et al., 1996, 2000a,b; Cubo et al., 2012; Montes et al., 2010; Starck and Chinsamy, 2002). Notably, the animals to which *Stenaulorhynchus* is most similar are all either large-bodied (*Proterosuchus*, *Alligator*) or bradymetabolic (*Anas*, mammals). In *Stenaulorhynchus*, the high depositional rates estimated in the first year of growth may be explained by size, metabolism, or a combination of both.

4.2. Histological comparison with other rhynchosaurs

The only other rhynchosaur femora described histologically are that of *Hyperodapedon*. Veiga et al. (in press) described a single femur from the Santa Maria 2 Sequence (Upper Triassic) of Brazil, which was sectioned only from fragments near the proximal end (UFRGS PV-0271-T). These exhibit a thin cortex vascularized by longitudinal primary osteons that decrease in number periosteally, similar to NHMUK PV R 36618. The primary tissues of that specimen were described as fibrolamellar based on osteocyte

Table 3
Periosteal deposition rates for parallel-fibered bone in the humeri, femora, and tibiae of living and extinct (denoted with †) tetrapods. *For Stenaulorhynchus*, deposition rates are given for the first year (1) and second through fifth years (2–5) separately.
Tableau 3
Taux de dépôt périostique pour l'os à fibres parallèles dans les humérus, les fémurs et les tibias des tétrapodes vivants et éteints (notée avec †). Pour *Stenaulorhynchus*, les taux de dépôt sont indiqués pour la première année (1) et de la deuxième à la cinquième années (2–5) séparément.

Clade	Taxon	Element	Deposition Rate (μm/d)	Study
Anura	*Nectophrynoides occidentalis*	Femur	0.52–0.62	Castanet et al., 2000a, b
Caudata	*Triturus cristatus*	Humerus	0.15–0.25	Francillon, 1979
Archosauromorpha	**†*Stenaulorhynchus***	**Femur (1)**	**14.78–45.33**	**This study**
		Femur (2–5)	**2.61–5.56**	
		Tibia (1)	**10.39–36.00**	
		Tibia (2–5)	**1.65–3.50**	
	†*Proterosuchus fergusi*	Humerus, Femur, Tibia	11.3	Botha-Brink and Smith, 2011
	†*Euparkeria capensis*	Humerus, Femur, Tibia	1.4	Botha-Brink and Smith, 2011
	Alligator mississippiensis	Femur	2.99–5.94	Roberts et al., 1988
		Femur	0.53–3.67	Woodward et al., 2014
		Tibia	0.21–2.76	Woodward et al., 2014
	†*Rhamphorhynchus*	Femur	2.5–5	Padian et al., 2004
	†*Masiakasaurus knopfleri*	Femur, tibia	~3	Lee and O'Connor, 2013
	Anas platyrhynchos	(several)	0.2–30	de Margerie et al., 2002
Chelonia	*Pelodiscus sinensis*	Tibia	0.39	Montes et al., 2007, 2010
	Emys orbicularis	Femur	0.25–0.37	Castanet, 1985
Lepidosauria	*Sphenodon punctatus*	Femur	0.28–0.36	Castanet et al., 1988
	Gallotia atlantica	Femur	0.30–0.45	Castanet and Baez, 1991
	G. galloti galloti	Femur	0.20–0.50	Castanet and Baez, 1991
	†*G. goliath*	Femur	0.18–0.74	Castanet and Baez, 1991
	G. stehlini	Femur	0.20–0.53	Castanet and Baez, 1991
	Lacerta viridis	Femur	0.14–0.56	Castanet, 1985
	Podarcis muralis	Tibia	0.15	Montes et al., 2007, 2010
	Varanus exanthematicus	Tibia	1.02	Montes et al., 2007, 2010
	V. niloticus	Tibia	0.8	Montes et al., 2007, 2010
	Zootoca vivipara	Tibia	0.22	Montes et al., 2007, 2010
Mammalia	*Macaca nemestrina*	Humerus	0.9–10.9 (usually ~2)	Newell-Morris and Sirianni, 1982
	Microcebus murinus	Tibia	3–8	Castanet et al., 2004
	Mus musculus	Tibia	4.08	Montes et al., 2007, 2010

shape and arrangement, and no growth marks were visible. Differences in femoral cortical thickness and growth mark presence between UFRGS PV-0271-T and NHMUK PV R 36618 partly reflect sampling location. In long bones, the cortex is always thickest at the mid-diaphysis and becomes much thinner towards the epiphyses. The mid-diaphysis also preserves the longest portion of the growth record, so fewer growth marks are visible at the ends of a bone.

Veiga et al. (in press) also described the mid-diaphyseal tibial histology of *T. sulcognathus* and *Hyperodapedon* from the Santa Maria 2 Sequence in Brazil. They found that the cortices of smaller individuals were composed of fibrolamellar bone with a significant woven-fibered component. These tissues were well vascularized by primary osteons that anastomosed extensively to form plexiform patterns. Larger individuals sometimes preserved similar tissue in the perimedullary region, but their cortices were mainly composed of parallel-fibered bone, poorly vascularized by longitudinal primary osteons, and with several LAGs or annuli (Veiga et al., in press). In the largest individuals, the mid-diaphyseal cortex was very thin relative to both the diameter and to the cancellous inner tissues, and perimedullary secondary osteons were common. Other elements preserved an EFS, but these were not visible in the tibiae sectioned. These taxa differ from NHMUK PV R 36618 in the presence of fibrolamellar bone and in the complexity of vascular canal patterns.

Mukherjee (2015) described femoral and tibial growth series from two species, *H. huxleyi* and *H. tikiensis*, from the Late Triassic Maleri Formation and Tiki Formation (respectively) of India. In both taxa, the inner cortex (internal to the first LAG) is composed entirely of woven-fibered or fibrolamellar bone. In *H. tikiensis*, this region is well vascularized by laminar or plexiform primary osteons. Porosity is much lower in *H. huxleyi*, but longitudinal primary osteons anastomose in all directions (Mukherjee, 2015). After the first year, zonal width and porosity decrease, parallel-fibered bone becomes progressively more common than fibrolamellar bone, and the primary osteons are arranged circumferentially or in radial rows (similar to NHMUK PV R 36618). The outer cortex of older individuals is nearly avascular. As in other rhynchosaurs, annuli and LAGs are present. In the femora and tibiae, annuli are more common in earlier years (e.g., Mukherjee, 2015; fig. 4A); these are often flanked by LAGs in the mid and outer cortex (e.g., Mukherjee, 2015; fig. 6C, D). No EFS is reported for either taxon, but growth in the outermost cortex has clearly slowed has down dramatically into regular cycles of parallel-fibered zones and lamellar annuli flanked by LAGs (e.g., Mukherjee, 2015; fig. 6B; note that our interpretation of this pattern is slightly differs from that author's). These taxa differ from NHMUK PV R 36618 in the presence of woven-fibered bone, the persistence of parallel-fibered bone in the outermost cortex, and in the density and complexity of vascular canal patterns. These differences are most notable in *H. tikiensis*; *H. huxleyi* likely grew slower based on fibrillar organization, canal density, and extent of vascular anastomoses (Mukherjee, 2015).

Two additional specimens warrant discussion. de Ricqlès et al. (2008) described the histology of two "rib" shafts of *Hyperodapedon* sp. (then *Scaphonyx*) from the Ischigualasto Formation (Upper Carnian) of Argentina. One had a typical rib lenticular cortical outline and histology, but the shape and histology of the other bone was so different that they questioned its identification. This specimen (MCZ FN 354-5, section 1.2.T) was larger and kidney-shaped, with a thick cortex. Its primary tissues were composed of parallel-fibered bone with distinct lamellar annuli ending in LAGs, and were much better vascularized than the other "rib", especially endosteally. In the inner cortex of this specimen, vascular canals anastomosed frequently to form a sub-plexiform pattern (de Ricqlès et al., 2008: plate 1, fig. 2). In *Stenaulorhynchus*, no other limb elements are kidney-shaped in cross-section at mid-diaphysis (SW, personal obs.). Given its cross-sectional shape and histology, this specimen may be a tibial mid-diaphysis rather than a rib.

The other noteworthy specimen is NMT RB154, a *Stenaulorhynchus* sp. limb bone mid-diaphysis illustrated by Sanchez et al. (2012: fig. 4E, F). Based on its histology and kidney shape in cross-section, it likely is also a tibia. This individual is smaller than NHMUK PV R 36618 (12.1 × 12.4 mm) and differs histologically in several ways. In NMT RB154, the cortical compacta is much thicker than the cancellous region. The primary cortex of NMT RB154 is comparably vascularized to the inner cortex of NHMUK PV R 36618, but has more radial and radially oblique anastomoses. Growth marks are present, but are less distinct than those of NHMUK PV R 36618. No information on the fibrillar organization is presented, and the sections are not illustrated at sufficient magnification to discern it. Both specimens have a small but distinct central medullary cavity.

4.3. Ontogenetic trends in rhynchosaur histology and growth

In both the femur and tibia of NHMUK PV R 36618, two thirds of the bone deposition occurred in the first year (SOM). The combination of an intense first year of growth, followed by sharp decreases in bone deposition rate in the second and sixth years of growth, suggests that the growth curve for this individual attenuated dramatically with age. In other words, NHMUK PV R 36618 experienced determinate growth that approached an upper asymptote after only a few years. In this specimen, the outermost LAGs are incompletely preserved around the circumference of the bone because of surface abrasion. Unfortunately, it is impossible to measure their circumferences or to calculate age-circumference or age-mass growth curves for this individual because of surface abrasion and taphonomic fracturing.

The transitions in *Stenaulorhynchus* bone deposition rates are coincident with histological changes. In NHMUK PV R 36618, femoral and tibial vascularity are highest internal to the first LAG, which is also the only region that preserves anastomoses. Canal density declines in years 2-5, and the bone tissue in the outermost zones is nearly avascular. This observation is consistent with previous studies that found a link between canal density and bone growth rate in a variety of amniotes (e.g., Cubo et al., 2012; Legendre et al., 2013). Similarly, the primary bone tissue of the innermost zone is mostly parallel-fibered. Moving periosteally, the tissues become progressively more lamellar. Previous studies have also shown that collagen fibers become more disorganized as bone deposition rate increases (e.g., Castanet et al., 2000a,b; de Margerie et al., 2002).

Other rhynchosaurs may also have grown in a similar manner. Veiga et al. (in press) interpreted all sampled specimens of *T. sulcognathus* as adults (post-reproductive maturity, and near the end of growth). However, post-cranial measurements establish that the holotype, UFRGS PV-232-T, is much smaller than the two referred specimens, PV-298-T and PV-290-T (Montefeltro et al., 2013). For example, the tibial mid-diaphysis of PV-232-T is half the diameter of PV-290-T and its humeral mid-diaphysis is two thirds the diameter of PV-290-T (Montefeltro et al., 2013; Veiga et al., in press). The largest and most robust specimen, PV-290-T, has more developed articular surfaces than the other specimens (Montefeltro et al., 2013). Their histology also supports interpretation as a partial ontogenetic series. PV-232-T is well vascularized in a plexiform pattern throughout the tibial cortex, and the transition from fibrolamellar to parallel-fibered bone occurs near the periosteal surface. In PV-290-T, the tibial cortex is poorly vascularized, the transition from fibrolamellar to parallel-fibered bone occurs in the innermost cortex, and secondary remodeling is much more extensive. PV-290-T does not preserve a tibia, but its humeral proximal diaphysis shows a mid-cortical transition in vascularization and fibrillar organization (Veiga et al., in press).

Mukherjee (2015) reported a nearly identical pattern of growth in *Hyperodapedon* from the Late Triassic of India. Both species experienced the greatest increase in bone circumference in the first year, during which they grew to approximately 1/3 adult size. The bone deposited in this time was woven-fibered or fibrolamellar bone and had both the greatest vascular density and the most complex vascular patterning. After this year, zonal width progressively decreased in size, the bone transitioned from woven- to parallel-fibered and ultimately to lamellar, and porosity decreased. The main difference between these species and the Brazilian taxa is that no EFS was reported in the Indian *Hyperodapedon* (Mukherjee, 2015).

Despite differences in fibrillar organization and vascular patterning, *Stenaulorhynchus* and the Upper Triassic rhynchosaurs share a common determinate growth pattern. The spacing between LAGs in all taxa sampled to date suggests faster initial growth lasting 1–2 growth seasons, followed by several years of dramatically slower growth, ultimately transitioning into an EFS in *Stenaulorhynchus* and the Brazilian taxa. An EFS was not found in the Indian taxa, but growth rates strongly attenuated late in life. In all taxa, decreased annual bone deposition is mirrored histologically by changes in fibrillar organization and vascularity. In the innermost zones, collagen fibers are more disorganized and canals are more numerous and better connected. As the growth zones attenuate in width, the fibers become lamellar and canals decrease in number and

connectivity. Because this general growth pattern is shared among several taxa, we disagree with Mukherjee (2015) and hypothesize that most (perhaps all) rhynchosaurs reached their upper growth asymptote before death (i.e., that they experienced determinate growth).

Among nonavian reptiles, determinate growth is known in a wide variety of taxa, including dinosaurs (e.g., Chinsamy, 1990; Erickson et al., 2004; Horner et al., 2009; Lee and O'Connor, 2013), pseudosuchian archosaurs (de Ricqlès et al., 2008; Tucker et al., 2007; Woodward et al., 2011), lepidosaurs (Bronikowski and Arnold, 1999; Castanet et al., 1988; Hugi and Sánchez-Villagra, 2012; Lailvaux et al., 2004), turtles (Congdon et al., 2001), and sauropterygians (Hugi et al., 2011; Klein, 2010a,b). It is also known in some fish (Okuda et al., 1998) and in all three extant amphibian clades (Haft and Franzen, 1996; Hanken, 1982; Martof, 1956; Woolbright, 1989). Determinate growth is not universal, and many taxa (especially among poikilotherms) do not commonly reach asymptotic size before death in the wild. However, we are not aware of any tetrapod species that does not attenuate growth toward an asymptote late in life. In this context, the determinate growth observed in *Stenaulorhynchus* and other rhynchosaurs is not surprising.

4.4. Long bone histological variation within non-archosauriform archosauromorpha

Despite sharing a similar determinate growth trajectory, rhynchosaurs varied somewhat histologically (at least based on tibial comparisons), and by extension, in their inferred relative growth rates. Of the taxa discussed here, *Stenaulorhynchus* shows numerous signs of slower growth compared to *Teyumbaita* and *Hyperodapedon* from Brazil and India. Unlike those taxa, it does not preserve woven-fibered or fibrolamellar bone, even in the innermost cortex (i.e., the tissues deposited when the animal was young and growing fastest). Compared to these taxa, *Stenaulorhynchus* is less vascularized throughout the cortex, and lacks anastomoses except early in life. Even then, the vascular patterns are never as complex or extensive as in the other taxa. The histology of the Argentinian *Hyperodapedon* is intermediate to these conditions: like NHMUK PV R 26618, it lacks woven-fibered bone, but it shares more complex vascular patterns with *Teyumbaita* and the other *Hyperodapedon*, at least earlier in ontogeny. Because the phylogenetic relationships within Hyperodapedontidae are poorly resolved (Fig. 1B) and there is variation even within the genus *Hyperodapedon*, the plesiomorphic condition for growth in this clade, and for Rhynchosauria, currently cannot be resolved.

Long bone histological variation is also present among the other non-archosauriform archosauromorphs. The protorosaur *Aenigmastropheus parringtoni* from the middle Late Permian of Tanzania showed histological signs of accelerated growth rates in the innermost humeral cortex, including moderately high levels of vascularization and woven-fibered bone tissue (Ezcurra et al., 2014). However, most of the cortex was composed of much slower-growing tissues (e.g., parallel-fibered or lamellar bone with infrequent canal anastomoses; Ezcurra et al., 2014), suggesting that it grew at much slower rates for most of its life. *Trilophosaurus buettneri* from the Upper Triassic of Texas, USA, deposited nearly avascular lamellar bone throughout ontogeny; its tissue suggests very slow growth similar to that of extant lepidosauromorphs (Werning and Irmis, 2011). Botha-Brink and Smith (2011) described the tibial histology of the close relative of archosauriforms *Prolacerta broomi*, and found poorly vascularized and only very weakly woven or parallel-fibered bone tissue, consistent with moderate growth rates.

The long bone microstructure of non-archosauriform archosauromorphs generally suggests slower growth compared to archosauriforms. All sampled taxa (including rhynchosaurs) deposited moderately to poorly vascularized parallel-fibered or lamellar bone for a significant portion of their ontogeny, and we agree with others (Botha-Brink and Smith, 2011; Cubo et al., 2012; Mukherjee, 2015) that this was likely the plesiomorphic condition for Archosauromorpha. However, among non-archosauriform archosauromorphs, only *H. tikiensis* (Mukherjee, 2015) and *Trilophosaurus buettneri* (Werning and Irmis, 2011), have been sampled sufficiently and systematically to the level to confidently address ontogenetic and interelemental variation in growth and histology and data for the latter have only been published in conference abstracts. Also, *Hyperodapedon* and *Stenaulorhynchus* are the only non-archosauriform archosauromorph taxa for which specimens from more than one locality have been sampled. Broader phylogenetic, ontogenetic, and regional sampling may reveal additional histological and physiological variation than is currently described.

5. Conclusions

The long bone histology of *S. stockleyi* suggests relatively slow growth compared to archosauriforms, saurischian dinosaurs, or birds, consistent with its phylogenetic position as a non-archosauriform archosauromorph. The sampled individual experienced much higher rates of bone deposition in its first year compared to subsequent years, which ultimately end in an EFS. These trends were concomitant with histological changes that also suggest slowing growth, such as increasing fibrillar organization and decreasing vascularity moving periosteally. Similar changes occur in the rhynchosaurs *T. sulcognathus*, *H. tikiensis*, and *H. huxleyi*, suggesting that rhynchosaurs in general experienced a short initial burst of faster growth, followed by an extended period of slow growth. The presence of attenuating LAGs and an EFS suggests asymptotic growth for this taxon, with maximum body size reached during the animal's lifetime. This is notably dissimilar to Archosauriformes and in particular bird-line archosaurs (especially saurischian dinosaurs), whose long bones show histological signs of sustained elevated growth lasting several years.

Histological variation among different rhynchosaur clades serves as a caution against inferring a common growth rate among closely related taxa, even when the overall shape of the growth curve is similar. Because Rhynchosauria as a clade was geographically widespread, had a temporal duration that lasted about 20 million years, and

was ecologically diverse, and because several rhynchosaur taxa (including *Stenaulorhynchus*) are known from partial ontogenetic series, they are an ideal group for continued studies of bone histology and growth.

Acknowledgments

This material is based upon work supported by the National Science Foundation under award numbers EAR-1250123 (to S.W.) and EAR-1337291 (Earth-Life Transitions; to Kenneth D. Angielczyk and S.J.N.), as well as the Jurassic Foundation (to S.W.). We thank Paul Barrett and Sandra Chapman at NHMUK for access to specimens and permission to sample histologically. We also thank the University of California Museum of Paleontology, University of Texas Vertebrate Paleontology Lab, and Stony Brook University for access to thin sectioning equipment, and Alan Turner, Timothy Bromage and the Hard Tissue Research Unit (New York University) for access to imaging equipment. We also thank our reviewers, Holly Woodward and Torsten Scheyer, and our editor, Michel Laurin, for their helpful comments that improved our manuscript.

Appendix A. Supplementary data

Supplementary data associated with this article can be found, in the online version, at http://dx.doi.org/10.1016/j.crpv.2015.03.004.

References

Benton, M.J., 1983. The Triassic reptile *Hyperodapedon* from Elgin: functional morphology and relationships. Phil. Trans. R. Soc. Lond. B 302, 605–717.

Benton, M.J., 1984. The relationships and early evolution of the Diapsida. Symp. Zool. Soc. Lond. 52, 575–596.

Botha-Brink, J., Smith, R.M.H., 2011. Osteohistology of the Triassic archosauromorphs *Prolacerta*, *Proterosuchus*, *Euparkeria*, and *Erythrosuchus* from the Karoo Basin of South Africa. J. Vertebr. Paleontol. 31, 1238–1254.

Bronikowski, A.M., Arnold, S.J., 1999. The evolutionary ecology of life history variation in the garter snake *Thamnophis elegans*. Ecol. 80, 2314–2325.

Castanet, J., 1985. La squelettochronologie chez les reptiles. I. Résultats expérimentaux sur la signification des marques de croissance squelettiques chez les lézards et les tortues (1). Ann. Sci. Nat. Zool., Paris 7, 23–40.

Castanet, J., Baez, M., 1991. Adaptation and evolution in *Gallotia* lizards from the Canary Islands: age, growth, maturity and longevity. Amphibia-Reptilia 12, 81–102.

Castanet, J., Newman, D.G., Saint Girons, H., 1988. Skeletochronological data on the growth, age, and population structure of the tuatara, *Sphenodon punctatus*, on Stephens and Lady Alice Islands, New Zealand. Herpetologica 44, 25–37.

Castanet, J., Grandin, A., Abourachid, A., de Ricqlès, A., 1996. Expression de la dynamique de croissance dans la structure de l'os périostique chez *Anas platyrhynchos*. C. R. Acad. Sci. Paris, Ser. III 319, 301–308.

Castanet, J., Pinto, S., Loth, M.-M., Lamotte, M., 2000a. Âge individuel, longévité et dynamique de croissance osseuse chez un amphibien vivipare, *Nectophrynoides occidentalis* (Anoure, Bufonidae). Ann. Sci. Nat. 21, 11–17.

Castanet, J., Rogers, K.C., Cubo, J., Jacques-Boisard, J., 2000b. Periosteal bone growth rates in extant ratites (ostriche and emu). Implications for assessing growth in dinosaurs. C. R. Acad. Sci. Paris, Ser. III 323, 543–550.

Castanet, J., Croci, S., Aujard, F., Perret, M., Cubo, J., de Margerie, E., 2004. Lines of arrested growth in bone and age estimation in a small primate: Microcebus murinus. J. Zool., Lond. 263, 31–39.

Chatterjee, S., 1974. A rhyncosaur from the Upper Triassic Maleri Formation of India. Phil. Trans. R. Soc. Lond. B 267, 209–261.

Chinsamy, A., 1990. Physiological implications of the bone histology of *Syntarsus rhodesiensis* (Saurischia: Theropoda). Palaeontol. Afr. 27, 77–82.

Chinsamy, A., Chiappe, L.M., Dodson, P., 1995. Mesozoic avian bone microstructure: physiological implications. Paleobiology 21, 561–574.

Congdon, J.D., Nagle, R.D., Kinney, O.M., van Loben Sels, R.C., 2001. Hypothesis of aging in a long-lived vertebrate, Blanding's turtle (Emydoidea blandingii). Exper. Gerontol. 36, 813–827.

Cox, C.B., 1991. The Pangaea dicynodont *Rechnisaurus* and the comparative biostratigraphy of Triassic dicynodonts faunas. Palaeontology 34, 767–784.

Cubo, J., Le Roy, N., Martinez-Maza, C., Montes, L., 2012. Paleohistological estimation of bone growth rate in extinct archosaurs. Paleobiology 38, 335–349.

de Buffrénil, V., Pascal, M., 1984. Croissance et morphogenèse postnatales de la mandibule du vison (*Mustela vison* Schreiber): données sur la dynamique et l'interprétation fonctionnelle des dépôts osseux mandibulaires. Can. J. Zool. 62, 2026–2037.

de Buffrénil, V., Clarac, R., Fau, M., Martin, S., Martin, B., Pellé, E., Laurin, M., 2015. Differentiation and growth of bone ornamentation in vertebrates: A comparative histological study among the Crocodylomorpha. J. Morphol. 276, 425–445.

de Margerie, E., Cubo, J., Castanet, J., 2002. Bone typology and growth rate: testing and quantifying 'Amprino's rule' in the mallard (*Anas platyrhynchos*). C. R. Biologies 325, 221–230.

de Ricqlès, A., 1976. On bone histology of fossil and living reptiles, with comments on its functional and evolutionary significance. In: Bellairs, A.d'A., Cox, C.B. (Eds.), Morphology and Biology of Reptiles. Academic Press, New York, pp. 123–151.

de Ricqlès, A.J., Padian, K., Horner, J.R., 2003. On the bone histology of some Triassic pseudosuchian archosaurs and related taxa. Ann. Paleontol. 89, 67–101.

de Ricqlès, A., Padian, K., Knoll, F., Horner, J.R., 2008. On the origin of high growth rates in archosaurs and their ancient relatives: complementary histological studies on Triassic archosauriforms and the problem of a "phylogenetic signal" in bone histology. Ann. Paleontol. 94, 57–76.

Dilkes, D.W., 1995. The rhynchosaur *Howesia browni* from the Lower Triassic of South Africa. Palaeontology 38, 665–685.

Dilkes, D.W., 1998. The Early Triassic rhynchosaur *Mesosuchus browni* and the interrelationships of basal archosauromorph reptiles. Phil. Trans. R. Soc. Lond. B 353, 501–541.

Enlow, D.H., 1969. The bone of reptiles. In: Gans, C., Bellairs, A.d'A., Parsons, T.S. (Eds.), Biology of the Reptilia, Vol. 1 Morphology A. Academic Press, London, pp. 45–80.

Enlow, D.H., Brown, S.O., 1957. A comparative histological study of fossil and recent bone tissues. Part II. Texas J. Sci. 9, 186–214.

Erickson, G.M., Makovicky, P.M., Currie, P.J., Norell, M.A., Yerby, S.A., Brochu, C.B., 2004. Gigantism and comparative life-history parameters of tyrannosaurid dinosaurs. Nature 430, 772–775.

Ezcurra, M.D., Scheyer, T.M., Butler, R.J., 2014. The origin and early evolution of Sauria: reassessing the Permian saurian fossil record and the timing of the crocodile-lizard divergence. PLoS ONE 9, e89165, http://dx.doi.org/10.1371/journal.pone.0089165.

Francillon, H., 1979. Étude expérimentale des marques de croissance sur les humérus et les fémurs de tritons crêtés (*Triturus cristatus cristatus* Laurenti) en relation avec la détermination de l'âge individuel. Acta Zool. (Stockh.) 60, 223–232.

Francillon-Vieillot, H., de Buffrénil, V., Castanet, J., Géraudie, J., Meunier, F.J., Sire, J.Y., Zylerberg, L., de Ricqlès, A., 1990. Microstructure and mineralization of vertebrate skeletal tissues. In: Carter, J.G. (Ed.), Skeletal biomineralization: patterns, processes and evolutionary trends, 1. Van Nostrand Reinhold, New York, pp. 471–530.

Griffin, C.T., Nesbitt, S.J., In revision. The femoral ontogeny and long bone histology of the Middle Triassic (?Late Anisian) dinosauriform *Asilisaurus kongwe* and implications for the growth of early dinosaurs. J. Vertebr. Paleontol.

Gross, W., 1934. Die Typen des mikroskopischen Knochenbaues bei fossilen Stegocephalen und Reptilien. Z. Anat. Entwicklungs. 203, 731–764.

Gower, D.J., 2003. Osteology of the early archosaurian reptile *Erythrosuchus africanus* Broom. Ann. South Afr. Mus. 110, 1–88.

Haft, J., Franzen, M., 1996. Freilandbeobachtungen, Verhalten und Nachzucht der São Tomé-Blindwühle *Schistometopum thomense* (Bocage, 1873). Herpetofauna 18, 5–11.

Hanken, J., 1982. Appendicular skeletal morphology in minute salamanders, genus *Thorius* (Amphibia: Plethodontidae): growth regulation, adult size determination, and natural variation. J. Morphol. 174, 57–77.

Haughton, S.H., 1932. On a collectionof Karroo vertebrates from Tanganyika Territory. Quart. J. Geol. Soc. 88, 634–671.
Horner, J.R., Padian, K., de Ricqlès, A., 2001. Comparative osteohistology of some embryonic and perinatal archosaurs: developmental and behavioral implications for dinosaurs. Paleobiology 27, 39–58.
Horner, J.R., de Ricqlès, A., Padian, K., Scheetz, R.D., 2009. Comparative long bone histology and growth of the "hypsilophodontid" dinosaurs *Orodromeus makelai*, *Dryosaurus altus*, and *Tenontosaurus tillettii* (Ornithischia: Euornithopoda). J. Vertebr. Paleontol. 29, 734–747.
Hugi, J., Sánchez-Villagra, M.R., 2012. Life history and skeletal adaptations in the Galapagos Marine Iguana (*Amblyrhynchus cristatus*) as reconstructed with bone histological data – A comparative study of iguanines. J. Herpetol. 36, 312–324.
Hugi, J., Scheyer, T.M., Sander, P.M., Klein, N., Sánchez-Villagra, M.R., 2011. Long bone microstructure gives new insights into the life of pachypleurosaurids from the Middle Triassic of Monte San Giorgio, Switzerland/Italy. C. R. Palevol 10, 413–426.
Klein, N., 2010a. Long bone histology of Sauropterygia from the Lower Muschelkalk of the Germanic Basin provides unexpected implications for phylogeny. PLoS ONE 5 (7), e11613.
Klein, N., 2010b. Long bone histology of Sauropterygia from the Lower Muschelkalk of the Germanic Basin, provides unexpected implications for phylogeny. PloS ONE, e11613.
Lailvaux, S.P., Herrel, A., VanHooydonck, B., Meyers, J.J., Irschick, D.J., 2004. Performance capacity, fighting tactics and the evolution of life-stage male morphs in the Green Anole lizard (*Anolis carolinensis*). Proc. Royal Soc. Lond. B 263, 559–566.
Lamm, E.-T., 2013. Preparation and sectioning of specimens. In: Padian, K., Lamm, E.-T. (Eds.), Bone histology of fossil tetrapods. University of California Press, Berkeley, pp. 55–160.
Lee, A., O'Connor, P.M., 2013. Bone histology confirms determinate growth and small body size in the noasaurid theropod *Masiakasaurus knopfleri*. J. Vertebr. Paleontol. 33, 865–876.
Legendre, L.J., Segalen, L., Cubo, J., 2013. Evidence for high bone growth rate in *Euparkeria* obtained using a new paleohistological inference model for the humerus. J. Vertebr. Paleontol. 33, 1343–1350.
Martof, B., 1956. Growth and development of the Green Frog, *Rana clamitans*, under natural conditions. Am. Midland Nat. 55, 101–117.
Montefeltro, F.C., Langer, M.C., Schultz, C.L., 2010. Cranial anatomy of a new genus of hyperodapedontine rhynchosaur (Diapsida, Archosauromorpha) from the Upper Triassic of southern Brazil. Earth Env. Sci. T. Roy. Soc. Edin. 101, 27–52.
Montefeltro, F.C., Bittencourt, J.S., Langer, M.C., Schultz, C.L., 2013. Postcranial anatomy of the hyperodapedontine rhynchosaur *Teyumbaita sulcognathus* (Azevedo and Schultz, 1987) from the Late Triassic of Southern Brazil. J. Vertebr. Paleontol. 33, 67–84.
Montes, L., Le Roy, N., Perret, M., de Buffrénil, V., Castanet, J., Cubo, J., 2007. Relationships between bone growth rate, body mass and resting metabolic rate in growing amniotes: a phylogenetic approach. Biol. J. Linn. Soc. 92, 63–76.
Montes, L., Castanet, J., Cubo, J., 2010. Relationship between bone growth rate and bone tissue organization in amniotes: first test of Amprino's rule in a phylogenetic context. An. Biol. 60, 25–41.
Mukherjee, D., 2015. New insights from bone microanatomy of the Late Triassic *Hyperodapedon* (Archosauromorpha, Rhynchosauria): implications for archosauromorph growth strategy. Palaeontology 58, 313–339.
Nesbitt, S.J., Barrett, P.M., Werning, S., Sidor, C.A., Charig, A.J., 2013. The oldest dinosaur? A Middle Triassic dinosauriform from Tanzania. Biol. Lett. 9, 20120949, http://dx.doi.org/10.1098/rsbl.2012.0949.
Nesbitt, S.J., Flynn, J.J., Pritchard, A.C., Parrish, J.M., Ranivoharimanana, L., Wyss., A.R., in revision. Postcranial osteology of *Azendohsaurus madagaskarensis* (?Middle to Upper Triassic, Isalo Group, Madagascar) and its systematic position among stem archosaur reptiles. Bull. Am. Mus. Nat. Hist.
Newell-Morris, L., Sirianni, J.E., 1982. Parameters of bone growth in the fetal and infant macaque (*Macaca nemestrina*) humerus as documented by trichromatic bone labels. In: Dixon, A.D., Sarnat, B.G. (Eds.), Factors and Mechanisms Influencing Bone Growth, Progress in Clinical & Biological Research 101. Alan R Liss, Inc, New York, pp. 243–258.
O'Leary, M.A., Kaufman, S.G., 2012. MorphoBank 3. 0: web application for morphological phylogenetics and taxonomy. http://www.morphobank.org
Okuda, N., Tayasu, I., Yanagisawa, Y., 1998. Determinate growth in a paternal mouthbrooding fish whose reproductive success is limited by buccal capacity. Evol. Ecol. 12, 681–699.
Padian, K., Horner, J.R., de Ricqlès, A., 2004. Growth in small dinosaurs and pterosaurs: the evolution of archosaurian growth strategies. J. Vertebr. Paleontol. 24, 555–571.
Peabody, F.E., 1961. Annual growth zones in living and fossil vertebrates. J. Morphol. 108, 11–62.
Roberts, E.D., Matlock, C.L., Joanen, T., McNease, L., Bowen, M., 1988. Bone morphometrics and tetracycline marking patterns in young growing American alligators (*Alligator mississippiensis*). J. Wildlife Dis. 24, 67–70.
Sanchez, S., Ahlberg, P.E., Trinajstic, K.M., Mirone, A., Tafforeau, P., 2012. Three-dimensional synchrotron virtual paleohistology: a new insight into the world of fossil bone microstructures. Microsc. Microanal. 18, 1095–1105.
Scheyer, T.M., Desojo, J.B., Cerda, I.A., 2014. Bone histology of phytosaur, aetosaur, and other archosauriform osteoderms (Eureptilia, Archosauromorpha). Anat. Rec. 297, 240–260.
Seitz, A.L.L., 1907. Vergleichende Studien über den mikroskopischen Knochenbau fossiler und rezenter Reptilien und dessen Bedeutung für das Wachstum und Umbildung des Knochengewebes im allgemeinen. Nova Acta. Abh. K. Leop. -Carol. Deutsch. Akad. Naturf. 87, 230–370.
Starck, J.M., Chinsamy, A., 2002. Bone microstructure and developmental plasticity in birds and other dinosaurs. J. Morphol. 254, 232–246.
Tucker, A.D., Limpus, C.J., McDonald, K.R., McCallum, H.R., 2007. Growth dynamics of freshwater crocodiles (*Crocodylus johnstoni*) in the Lynd River, Queensland. Austral. J. Zool. 54, 409–415.
Veiga, F., Soares, M.B., Sayão, J.M., in press. Osteohistology of hyperodapedontine rhynchosaurs from the Upper Triassic of southern Brazil. Acta Palaeontol. Pol. Online in advance of print. doi: 10.4202/app.00074.2014.
von Huene, F., 1938. Stenaulorhynchus, ein Rhynchosauride der ostafrikanischen Obertrias. Nova Acta Leopoldina (N.F.) 6, 83–112.
Wells, J.W., 1963. Coral growth and geochronometry. Nature 197, 948–950.
Werning, S.A., Unpublished PhD Dissertation 2013. Evolution of Bone Histological Characters in Amniotes and the Implications for the Evolution of Growth and Metabolism. University of California, Berkeley.
Werning, S., Irmis, R.B., 2011. Reconstructing the ontogeny of the Triassic basal archosauromorph *Trilophosaurus* using bone histology and limb bone morphometrics. Program and Abstracts, 70th Annual Meeting. Soc. Vertebr. Paleontol., 185A–186A.
Werning, S., Irmis, R.B., Nesbitt, S.J., Smith, N.D., Turner, A.H., Padian, K., 2011. Archosauromorph bone histology reveals early evolution of elevated growth and metabolic rates. Ameghiniana 48, R74–R75.
Woodward, H.N., Horner, J.R., Farlow, J.O., 2011. Osteohistological evidence for determinate growth in the American Alligator. J. Herpetol. 45, 339–342.
Woodward, H.N., Horner, J.R., Farlow, J.O., 2014. Quantification of intraskeletal histovariability in *Alligator mississippiensis* and implications for vertebrate osteohistology. Peer J. 2, e422, http://dx.doi.org/10.7717/peerj.422.
Woolbright, L.L., 1989. Sexual dimorphism in *Eleutherodactylus coqui*: selection pressures and growth rates. Herpetologica 45, 68–74.